

# Quantification of entanglement with Siamese convolutional neural networks

Jarosław Pawłowski<sup>1,\*</sup> and Mateusz Krawczyk<sup>1</sup>

<sup>1</sup>Department of Theoretical Physics, Wrocław University of Science and Technology, Wybrzeże Wyspiańskiego 27, 50-370 Wrocław, Poland

\*jaroslaw.pawlowski@pwr.edu.pl

## ABSTRACT

Quantum entanglement is a fundamental property commonly used in various quantum information protocols and algorithms. Nonetheless, the problem of quantifying entanglement has still not reached general solution for systems larger than two qubits. In this paper, we investigate the possibility of detecting entanglement with the use of the supervised machine learning method, namely the deep convolutional neural networks. We build a model consisting of convolutional layers, which is able to recognize and predict the presence of entanglement for any bipartition of the given multi-qubit system. We demonstrate that training our model on synthetically generated datasets collecting random density matrices, which either include or exclude challenging positive-under-partial-transposition entangled states (PPTES), leads to the different accuracy of the model and its possibility to detect such states. Moreover, it is shown that enforcing entanglement-preserving symmetry operations (local operations on qubit or permutations of qubits) by using triple Siamese network, can significantly increase the model performance and ability to generalize on types of states not seen during the training stage. We perform numerical calculations for 3,4 and 5-qubit systems, therefore proving the scalability of the proposed approach.

## Introduction

Modern deep learning (DL) architectures has enabled unprecedented achievements in various domains like computer vision or natural language processing. Convolutional neural networks (CNNs) with many hidden layers and complex network structure are extremely powerful in feature learning enabling automatic extraction of the most optimal features. Deep CNNs easily outperform classical algorithms in image classification<sup>1</sup>, object detection<sup>2,3</sup>, or face recognition tasks<sup>4</sup>. In physics, one natural application of DL involves the study of quantum many-body systems<sup>5-8</sup>, where the extreme complexity of many-body states often makes theoretical analysis intractable. Nonetheless, employment of machine learning (ML) in physics for entangled state representations is typically focused on more traditional architectures such as Boltzmann machines<sup>7,9</sup> or fully connected neural networks<sup>10</sup>. However, there are recent signals that deep convolutional and recurrent networks, can better represent highly entangled quantum systems<sup>11,12</sup>. Therefore, it is worth trying more modern architectures, which are closer to the state-of-the-art approaches in DL, to study entanglement.

Entanglement is a fundamental feature of quantum physics, where the correlation between subsystems (i.e particles) cannot be described within a *local* classical model. In quantum information theory, entanglement is regarded as an important resource in achieving various tasks, such as quantum computation, cryptography, and teleportation. Simultaneously, the problem of quantifying entanglement has not reached a general solution for systems larger than two qubits.<sup>13,14</sup> There exist analytic criteria for separability of a given mixed state which are either sufficient and necessary, but not practically usable (require minimization); or easy to use, but not conclusive<sup>13</sup>. One of the criterion of separability, which can be considered is PPT (positive under partial transpose) criterion<sup>15</sup>. It is based on the idea, that having density matrix partially transposed for a given bipartition, one can determine separability by simply looking at the eigenvalues of this matrix. Namely, if all eigenvalues are positive, then the state is separable in the given bipartition. However, in case of systems larger than two qubits it is only necessary condition of separability – there are no separable states, which have negative eigenvalues, but it is not sufficient condition – there exist mixed states, which are entangled although they are PPT. Such states are called PPT entangled states (PPTES). Similarly, all other operationally feasible analytic criteria provide partial solutions only.

An interesting idea in this area is to implement neural networks on a quantum computer<sup>16,17</sup> and thus create a bridge between DL and quantum computing<sup>18</sup>, leading to exponential speedup in training deep neural networks<sup>17</sup>. Recently discovered quantum convolutional neural networks<sup>19</sup> allow their efficient training and implementation on realistic quantum devices. Such networks can be used for efficient entanglement detection in multi-qubit systems<sup>20</sup>, as well as for solving different classes of quantum many-body problems such as quantum phase recognition<sup>19</sup>. ML can also be applied to an important problem in quantum algorithm design, the automatic optimization of large unitary matrices into sequences of two-qubit gates<sup>21</sup>.

Entanglement can also assist ML image classifiers by compressing image and thus reducing computational resources needed<sup>22</sup>.

Proposed studies will attempt to quantify entanglement using modern DL architectures and confront it with traditional analytic entanglement metrics. The first applications of advanced DL architectures to such problems, e.g. using unsupervised deep-learning to detect quantum states are already appearing<sup>23</sup>. In this approach we propose a similar idea but aim to solve more general problem of precise entanglement quantifying by predicting entanglement for each bipartition in a system. In this sense our model will predict vector of probabilities that quantifies entanglement distribution in the system, rather than just a single entanglement metric. Our method try to deal with more general quantum systems in classifying PPTES, i.e. in situations where the PPT criterion fails, and one cannot obtain reliable labels for supervised learning, than in approach that utilise multi-layer perception networks<sup>10</sup>. We also obtain better results than using classical, non-neural ML supervised algorithms<sup>24,25</sup>.

## Quantum entanglement

Before discussing the introduced methods for quantification of entanglement in a given  $n$ -qubit quantum system, let us introduce basic concepts and definitions used when discussing this phenomenon. The foundations of quantum mechanics state that in order to describe a system that forms a  $n$ -qubit register, one must define a  $2^n$ -dimensional state space (known as the Hilbert space). The most convenient (and general) way to describe these multi-qubit systems is to construct a density matrix:

$$\rho = \sum_i p_i |\psi_i\rangle \langle \psi_i|, \quad (1)$$

where  $p_i$  is a probability that the system is in a given state  $|\psi_i\rangle$ . Therefore, in this approach quantum space is represented by a mixture of states, or in other words a mixed state. However, if only one state is used to determine the whole system, then it is said, that it is a pure state. In such case the density matrix is reduced to the outer product of a state vector  $|\psi\rangle$  with itself  $\rho = |\psi\rangle \langle \psi|$ .

Having complex system, i.e., a system consisting of at least 2 qubits, one can define a separable state as the one, that can be separated to a tensor product of sub-system states. This definition is valid in case of pure states, however, it has to be extended to capture also mixed states. In the latter case, the bi-separable mixed state can be written as:

$$\rho_{AB} = \sum_i p_i \rho_A^i \otimes \rho_B^i, \quad (2)$$

where  $\sum_i p_i = 1$ , while  $\{\rho_A^i\}$  and  $\{\rho_B^i\}$  are the density matrices representing states of the corresponding sub-systems  $A$  and  $B$ . If the mixed state cannot be represented as such a convex sum ( $p_i \geq 0$ ) of product states, then the state is entangled.

In general, determining separability of a given state using the above-mentioned definition is a non-trivial problem.<sup>13</sup> Therefore, many different criteria have been constructed to decide whether a state is entangled. One noteworthy example is the negativity<sup>26</sup> metric, which is defined as follows:

$$Neg(\rho_{AB}) = \sum_{\lambda_i < 0} |\lambda_i|, \quad (3)$$

where  $\lambda_i$  are the negative eigenvalues of the partially transposed density matrix  $\rho^{TB}$  associated with the given bipartition  $A|B$  of the whole system. The partial transpose operation for its density matrix  $\rho_{AB} = \sum_{i,j,r,s} a_{i,r} a_{j,s}^* |i\rangle_A \langle j|_A \otimes |r\rangle_B \langle s|_B$ , with respect to the subsystem  $B$  is defined as:

$$\rho^{TB} = \sum_{i,j,r,s} a_{i,r} a_{j,s}^* |i\rangle_A \langle j|_A \otimes (|r\rangle_B \langle s|_B)^T = \sum_{i,j,r,s} a_{i,r} a_{j,s}^* |i\rangle_A \langle j|_A \otimes |s\rangle_B \langle r|_B. \quad (4)$$

The negativity metric  $Neg(\cdot)$  is based on the PPT separability criterion.<sup>27,28</sup> It states, that non-negative eigenvalues of the partially transposed density matrix are the necessary condition of separability. However, it is the sufficient condition only for  $2 \times 2$  or  $2 \times 3$  systems. In case of larger systems, one can be certain that if the negativity is larger than zero (NPT states), then the state is entangled. On the other hand, if the negativity is equal to zero (PPT states) it is not always true that the state is separable, i.e. we may have PPTES.

There exists some other methods of calculating entanglement, for instance entanglement of formation or entanglement witnesses, however they are far more complex (time-consuming) because they require optimization in high-dimensional spaces<sup>29-31</sup>, and therefore impractical to use in case of large datasets. All in all, one arrives with analytical methods which are either hard to calculate or sufficient only for pure states or low-dimensional mixed states. On the other hand, there exist numerical algorithms, which are able to quantify the entanglement after a finite time with a desired precision<sup>32-34</sup>. That is why, artificial neural networks, which are also approximate numerical methods, are supposed to cope with this task.

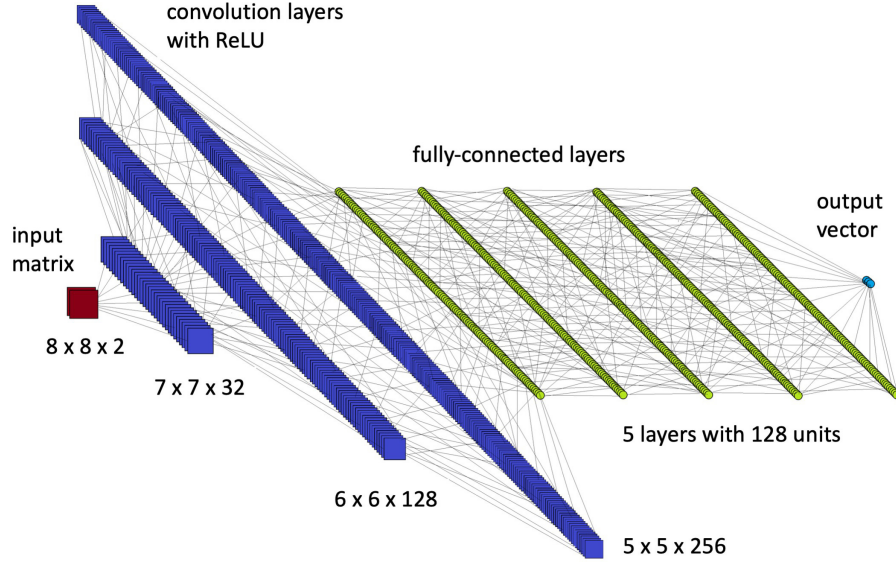


**Figure 1.** Neural network architecture for 3-qubit input density matrix (red): CNN backbone with three convolutional layers, each of  $2 \times 2$  kernel (dark blue blocks); five fully-connected layers (green blocks); and finally, 3-element output vector quantifying entanglement in three possible bipartitions (light blue).

## Neural network architectures

Detecting quantum entanglement in many-qubit systems is inseparably connected with analyzing the quantum state of the system, which is represented by a density matrix. The most natural concept of a neural network designed to process such an input (in a form of finite two-dimensional array) is a convolutional neural network (CNN). This type of ML model has already proved its efficiency dealing with quantum entangled systems.<sup>11, 35–38</sup>

### Deep convolutional networks

In this paper, we propose to use CNN as a feature extracting backbone followed by fully-connected classification layers. The network architecture is defined as follows. The input layer has size  $K \times K \times 2$ , where  $K$  is the Hilbert space dimension and the density matrix is split into the two channels by taking the real and the imaginary part separately. Subsequently, there are three convolutional layers with ReLU activation functions, each with kernel of size  $2 \times 2$ , and the number of channels in the  $i$ -th layer  $c_i = \lfloor r_i c_{i-1} \rfloor$ . Here, the  $r_i = \sqrt{r_{i-1}}$  parameter is the layers increase ratio initialized with  $r_1 = 16$ , and  $\lfloor \cdot \rfloor$  denotes floor operation. Convolutional layers are followed by five fully-connected layers with 128 units each and ReLU activation functions. Finally,  $m$ -units output vector with sigmoid activation functions is used, where  $m$  corresponds to the number of possible bipartitions in the  $N$  qubits system. The exemplary architecture of the CNN model for 3-qubit system is presented in Fig. 1.

The network is trained in a supervised manner. To evaluate the loss function we use binary cross entropy averaged over all possible bipartitions:

$$\mathcal{L}_{\text{CNN}} = L_{\text{BCE}}(\mathbf{p}(\boldsymbol{\rho}), \mathbf{q}) = -\frac{1}{mn} \sum_j^m \sum_i^n q_{ij} \log(p_j(\rho_i)) + (1 - q_{ij}) \log(1 - p_j(\rho_i)), \quad (5)$$

where  $m$  is the number of bipartitions,  $n$  is the batch size,  $q_{ij}$  is the label for the  $j$ -th bipartition of the given state  $\rho_i$  (with 0 meaning separable, and 1 – entangled bipartition), and  $p_j(\rho_i)$  is the predicted probability that  $\rho_i$  has parts for  $j$ -th bipartition entangled.

### Siamese networks

Entanglement should be invariant to local operations taken on separate qubits. In other words, applying single qubits rotations or phase modification do not influence the entanglement between different qubits. Moreover, permutations of the qubits in the system also should not have any impact on the entanglement quantification. Having those two facts in mind, we propose to extend the CNN into triple Siamese neural network, to force the model to be immune for such symmetry operations, and thus improve its robustness. Specifically, in this approach instead of having only one density matrix on the input, we augment it into

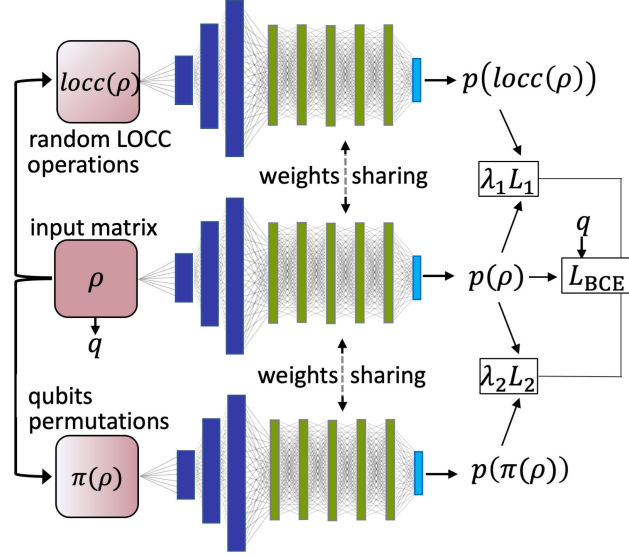


**Figure 2.** Architecture of the triple Siamese network, where each subnetwork (being the CNN from Fig. 1) is fed by a different input (original or transformed), but share the same network parameters (weights).

three matrices, which are processed parallelly. The characteristic is that each subnetwork is an exact copy of the original CNN but with the model weights *shared* between them – see Fig. 2. The first input is the original matrix, the second one represents the original state with an extra random local operations (LOCC) applied to each qubit, and the third one corresponds to the density matrix, which is permuted with respect to randomly selected qubits. Hence, now the loss for a given batch is defined as follows:

$$\mathcal{L}_{\text{siam}} = L_{\text{BCE}}(\mathbf{p}(\boldsymbol{\rho}), \mathbf{q}) + \lambda_1 \frac{1}{mn} \sum_j^m \sum_i^n |p_j(\rho_i) - p_j(\text{locc}(\rho_i))| + \lambda_2 \frac{1}{mn} \sum_{k=\pi(j)}^m \sum_i^n |p_j(\rho_i) - p_k(\pi(\rho_i))|, \quad (6)$$

where by  $\text{locc}(\rho_i)$  we denote some random LOCC operation on state  $\rho_i$ ,  $\pi(\rho_i)$  is the permutation of state  $\rho_i$  chosen independently for a given batch, and  $\lambda_1, \lambda_2$  are hyperparameters which allow to adjust the influence of such extending loss functions. One important remark is, that permutation  $\pi$  can rearrange the output vector in case of certain bipartitions. For example, 3-qubit permutation  $\pi = (1)(23)$  does not change the predicted probability of entanglement for the bipartition (1|23). Contrarily, the same permutation switches the probabilities for the other two bipartitions (2|13 and 3|12). Therefore, corresponding indexes must be selected carefully, which we denoted by writing  $k = \pi(j)$ .

## Training data generation

The most crucial thing to train a ML model is to have well balanced and diversified dataset. Thus, in order to achieve this goal, we propose various methods of density matrices generation, that will be used to build synthetic dataset for training our neural network models.

Two main techniques were used to generate pure random states. The first idea is to use a quantum circuit model that contains local single-qubit gates  $U$  that randomize separate qubits, and random number of two-qubit controlled gates  $CU$ , that can entangle qubits. The  $CU$  gates are put to random pairs of qubits. Combining these two types of quantum gates with their appropriate parameters (angles), one can obtain a suitable generator of pure states, both entangled and separable ones. The detailed parametrization of the gates and circuit organization can be found in the Supplementary Materials. Example of a 3-qubit circuit generated by this method is presented in Fig. 3. The second idea of generating random pure states is based on sampling from the uniform Haar measure<sup>39</sup> described in the Supplementary Materials.

Having these two methods, one can suspect that using both of them produces the sufficiently diversified dataset of the pure state vectors and consequently density matrices. However, apart from them, we also included three specific types of quantum states, which may hardly occur when using both procedures. Namely, using circuit approach we intentionally generate pure separable states (here  $CU$  gates are absent in the circuit), the GHZ state, and the W state<sup>40</sup>, each of them being locally randomized with the  $U$  gates. It is obvious, that having only pure states included in training dataset may result in missing the possibility of detecting mixed states. That is why, we should also think of generating such states straight from the definition of

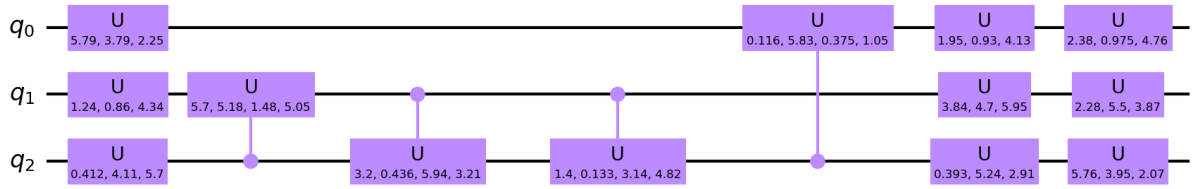


**Figure 3.** Example of a circuit generating a 3-qubit random state. It consists of  $U$  and  $CU$  gates (violet blocks) with random parameters written in the each block.

a mixed state:

$$\rho = \sum_i^d p_i |\psi_i\rangle \langle \psi_i|, \quad (7)$$

where for training purposes we select  $d$  at random over the interval  $[2, 2^N]$ , and  $N$  is a number of qubits. In this naïve method one simply mix many pure states  $|\psi_i\rangle$  with random probabilities  $p_i$ . However, to have as diversified dataset as possible, we also use the second method of generating mixed states:

$$\rho_{AB} = \text{tr}_C(|\Psi_{ABC}\rangle \langle \Psi_{ABC}|), \quad (8)$$

with a partial trace operation  $\text{tr}_C(\cdot)$ . Namely, we generate a larger pure system  $|\Psi_{ABC}\rangle$  and trace out some part of it (subspace  $C$ ), until the desired size of the system  $AB$  is achieved. This way, if the global space  $ABC$  is entangled, one can be sure that the reduced density matrix  $\rho_{AB}$  is mixed.

To train a neural network in a supervised learning scheme one needs to have labels  $q$  – see Fig. 2, which classify each bipartition of the system in a given state as entangled or separable. Then, each state  $x_i$  is labeled by a binary vector  $q_{ij}$ , where subsequent elements  $j$  encode presence of entanglement for the given bipartition. In case of pure states we calculate the negativity measure (Eq. 3) for each bipartition and mark it accordingly to its value: if  $Neg = 0$ , it is marked as separable, while if  $Neg > 0$  it is marked as entangled. While in case of mixed states, where it is not guaranteed that negativity measure distinguishes separable and entangled states, we either generate states that are separable (by definition) or entangled (by taking only NPT, i.e. where the negativity is conclusive), or in case of PPT we propose three different strategies for labeling unknown states. This latter group is important because it contains PPTES, and therefore allows to train a model to capture them.

The most naïve strategy is based on negativity metric and simply labels mixed states accordingly to the  $Neg$  value – we will call this strategy as *negativity labeled*. However, main problem with this approach is that it may falsely label mixed PPT states, i.e. where the criterion is inconclusive. That is why we introduce a second strategy called *verified*, where the PPT states are simply excluded from the data. The main disadvantage of such a solution is that it automatically excludes all of mixed separable states. To minimize this drawback, we supplement dataset by generating them straight from the definition. Finally, we propose a solution which extends the second method in a way that PPT states are not excluded, but an additional labeling criterion is applied to them. It verifies if the qubits from different partitions are connected by a controlled gate  $CU$  (that may introduce entanglement) in generation circuit, or not. We call this third strategy as *weakly labeled* because there is no guarantee that such labels are always correct. Further descriptions for all of these three strategies can be found in the Supplementary Materials.

Having defined various methods for generation of pure and mixed states together with three different strategies for labeling mixed states we have generated training datasets. They are summarized in Table 1, along with the number of generated states for each group. In total, we have synthesized three training sets, each with the same structure of the pure (100 000 states) and mixed separable (80 000 states), but with different strategies for labeling mixed entangled (150 000 states). In order to correctly evaluate the model, apart from the training sets, the validation and test sets were also created. The validation set is generated with the same structure as the *verified* training dataset, but with 10 times smaller number of examples, i.e. 33 000 states generated. Next, we defined two test datasets for pure (30 000 states) and mixed states separately. The latter contains 20 000 separable states, and 20 000 entangled containing NPT states only (*verified* strategy), generated both from the definition (Eq. 7) and using partial trace (Eq. 8). Therefore, test dataset contains only the correctly labeled states. Further details on states generation can be found in the Supplementary Materials.

Since the main reason of creating the artificial classifier is to have an ability to detect not only NPT entangled states but also PPTES, thus additionally we generate 3 separate test datasets, each containing 10 000 well defined PPTES of different type. Precisely, the first PPTES test set includes  $2 \otimes 4$  PPTES introduced by Horodeccy<sup>15</sup> and then generalized to  $N$ -qubits,  $2 \otimes 2^{N-1}$

state type	generating method	labeling method	amount
pure separable	circuit with random 1-qubit gates only (separable circuit)	negativity	40 000
pure entangled	random circuits, including W and GHZ, and sampling from the Haar measure	negativity	60 000
mixed separable	separable circuit then formula (SM4), and Kronecker product of mixed 1-qubit	by definition	60 000 + 20 000
mixed entangled	from the definition (7), and using partial trace (8)	3 strategies: <i>negativity</i> , <i>verified</i> , <i>weakly</i>	90 000 + 60 000

**Table 1.** Training datasets composition. All three sets have the same structure of pure and mixed separable states, but have different strategies for labeling mixed entangled states.

dimensional states<sup>41</sup>. The second test set is composed of fully PPT entangled states proposed by Acin et al.<sup>42</sup> And the third one is generated with the use of unextendible product basis (UPB)<sup>43</sup>, with similar approach being described by Ma et al.<sup>10</sup>. All of these states are furtherly randomized by applying local operations to the separate qubits.

## Results

After we have defined the deep neural network models and generated the labeled training and test sets, we can move on to training and then testing our models. To verify the models fidelity we used the standard accuracy metric, which is defined as follows:

$$Acc = \frac{1}{mn} \sum_{i=1}^m TP_i + TN_i, \quad (9)$$

where  $m$  is the number of possible bipartitions,  $TP_i$  and  $TN_i$  represent the number of true positive (entangled classified as entangled) and true negative (separable classified as separable) examples for a given bipartition  $i$ , and  $n$  is the total number of samples in the test datasets.

We also optimized the models architecture hyperparameters by training them on the *weakly labeled* training set and evaluating on the validation set – discussion can be found in the Supplementary Materials. Results show that the most efficient architecture is the network (CNN or Siamese) with 3 convolutional layers and kernel size equal to  $2 \times 2$ .

### Three-qubit system

Let us start with the results for the smallest configuration where nontrivial entanglement relations may occur, i.e. 3-qubit system. In Tables 2 and 3 there are presented results for CNN and Siamese network models, trained on the all three training sets: *negativity labeled*, *weakly labeled*, and *verified*. The accuracy was calculated for the all generated test sets: with pure states, mixed states, and with various PPTES classes.

The first thing, that one can notice, is that both models work pretty well in case of pure states, reaching accuracies over 97%. However, they do not detect all of the mixed states. It is especially visible when using *weakly labeled* training set. The

Training sets	Pure states	Mixed states	Horodecki PPTES	UPB PPTES	Acin PPTES
negativity labeled	97,39	92,82	99,72	84,67	3,11
weakly labeled	97,56	85,33	100,00	92,65	37,69
verified	97,78	92,59	99,77	88,96	12,54

**Table 2.** Averaged bipartite entanglement detection accuracy for 3-qubit system using CNN model for different training sets, and test sets together with the various classes of PPTES.

Training sets	Pure states	Mixed states	Horodecki PPTES	UPB PPTES	Acin PPTES
negativity labeled	97,94	93,14	99,80	95,94	0,74
weakly labeled	97,89	89,69	100,00	95,60	36,75
verified	97,76	93,39	99,97	94,94	5,25

**Table 3.** Same as in Table 2, but with Siamese network model.

model trained on such data has a bit lower accuracy of detecting mixed states, however, it is better suited to classify various PPTES – in particular it is able to recognize at least some PPTES of the Acin class.

When it comes to comparing CNN and Siamese network (Table 2 vs. 3), one can see the advantage of the Siamese model in recognizing mixed states. It is clear that it generally gives better results than CNN, but the greatest profit from using this architecture is by its ability to detect UPB states. In this case, independently of the used training set, we obtained quite high accuracy. It is worth to remind here, that all models were trained on the datasets, which do not directly include given classes of PPTES. This means, that the models can generalize well on cases of Horodecki and UPB states – the best generalization is observed for the Siamese network trained on the *weakly labeled* set. The worse tendency to generalize is for CNN model and *negativity* labeled set, which is natural because this set learns that PPTES are not entangled. Interestingly, the use of Siamese architecture restores the model’s ability to detect these states and makes the results similar to those when trained on *verified* one. Unfortunately, the use of Siamese architecture has not improved detection of the Acin class, giving even a slightly reduced accuracy.

In contrast, in Table 4 there are presented accuracies for the models from Table 3 but additionally retrained, using extra 5 epochs, on the extended training sets which includes 20 000 UPB and 30 000 of randomized Acin PPTES. Here we can observe that retraining model on such extended dataset, allows the network to detect nearly all PPTES. However, in case of *weakly labeled* training set it comes with the reduced accuracy of mixed states detection. On the other hand, one can see now that the most optimal method of labeling the training set is the *verified* method, where no accidentally generated PPTES are included. Nonetheless, one should realize that including such PPTES in the training set is only applicable for 3-qubit systems, since the states generated from the UPB and Acin classes are defined for  $8 \times 8$  dimensional spaces only.

When thinking about PPTES detection, one can also come with slightly modified approach. Namely, as per definition, negativity value for PPT state is equal to 0. Moreover, as stated before, it is guaranteed that each NPT state, for which the negativity is larger than 0, is entangled. Therefore, we also tested a combined classifier, which firstly calculates the negativity value for each bipartition of the given state, and then, if and only if it is equal to 0, use the neural network to predict the actual entanglement. This way, one can easily increase the accuracy of the classifier, simultaneously maintaining its ability to detect PPTES. Outcomes of such an approach are presented in Table 5. It is visible, that now the classifier can detect nearly all pure states as well as majority of the mixed states. Obviously, one can get further the 100% accuracy of the entanglement detection in the pure states, simply by determining the purity first, and then calculating some well specified measure for pure states (e.g. von Neumann entropy could be used).

Additionally, we collect the model prediction results for special families of GHZ and W states. Accuracy calculated separately for GHZ and W states reaches 98% and 92% respectively for bipartite entanglements detection in case of the CNN model, and 99% and 97% for the Siamese CNN model. Presented results are for training performed on the *negativity labeled* dataset. Results for the other datasets are comparable in accuracy.

### Scaling to larger systems

Presented results for three qubits are promising, but only by scaling the models to larger systems where analytical methods can hardly be used will prove the usability of the ML approach. To do so, we trained the CNN and Siamese network for 4- and 5-qubit systems. The architecture of these models are equivalent to the 3-qubit model. The only difference is the size of the input density matrix and the size of the output vector  $m$  (number of possible bipartitions), which is equal to 7 for 4 qubits (i.e. three  $2|2$  qubits bipartitions, and four  $1|3$  qubits bipartitions) and 15 in case of 5 qubits system.

In Fig. 4 there are presented results of bipartite entanglement detection for different system sizes. It is visible, that Siamese network provides higher accuracy not only for 3-qubit systems but also for higher dimensional spaces. What is interesting, the accuracy of the model seems to grow with the system size in case of mixed states. In particular, there is a large gap between accuracy for 3- and 4-qubit systems. However, one should recall, that in case of 3 qubits there is also noticeable difference in accuracy for mixed states, depending on the training set – see Table 3. If we look at the results for the *verified* training set presented in Fig. 5, we observe that now the gap between the accuracy of the 3 and 4 qubits models is definitely smaller than before, for *weakly labeled* set presented in Fig. 4(b).

However, one can notice, that while accuracy for the 3-qubit system increased, the accuracy for 4 and 5 qubits decreased by

Training sets	Pure states	Mixed states	Horodecki PPTES	UPB PPTES	Acin PPTES
negativity labeled	98,03	92,80	100,00	100,00	81,57
weakly labeled	98,22	86,45	100,00	100,00	89,33
verified	98,26	93,14	99,96	99,75	89,55

**Table 4.** Averaged bipartite entanglement detection accuracy for 3-qubit system with the Siamese network model trained on different datasets and then retrained on datasets containing UPB and Acin PPTES.

Training sets	Pure states	Mixed states
negativity labeled	99,87	97,64
weakly labeled	99,57	93,43
verified	99,60	96,81

**Table 5.** Averaged bipartite entanglement detection accuracy for 3-qubit system with Siamese network model combined with a negativity metric used first to sort out NPT states. Results for PPTES are the same as in Table 3.

approximate 1% for training on the *verified* dataset. Further analysis showed that the *verified* training dataset gives the best results only in case of 3 qubits, while the *weakly labeled* is better for larger systems. The detailed discussion with possible explanation can be found in the Supplementary Materials.

Finally, combining the predictions of the Siamese network with negativity used to sort out NPT states, as proposed for 3 qubits, one can obtain the classifier, which accuracy of bipartite entanglement detection for 5-qubit mixed states reaches 99.1%, as presented in Fig. 6.

## Discussion

The main problem with building a general classifier of entanglement in quantum states is a lack of reliable method for labeling entanglement of mixed states. If we label some states with mistakes, the ML methods may learn the mistakes as well. However, we were able to show that if we use a properly diversified training dataset, we can force the model to generalize correctly to capture some PPTES even if they have not been labeled correctly. This effect can even be strengthened if we use the architecture of Siamese networks, which forces the model to respect the system symmetries that do not change the entanglement configuration (LOCC or respective permutations). Improved model efficiency through the use of Siamese networks shows the possible direction for development of ML models for describing physical systems with their inherent symmetries.

During the research, in addition to CNN and CNN in triple-Siamese configuration, we also tested other neural network architectures. However, both generic multi-layer fully-connected networks, as well as more advanced tensor networks<sup>44</sup>, used

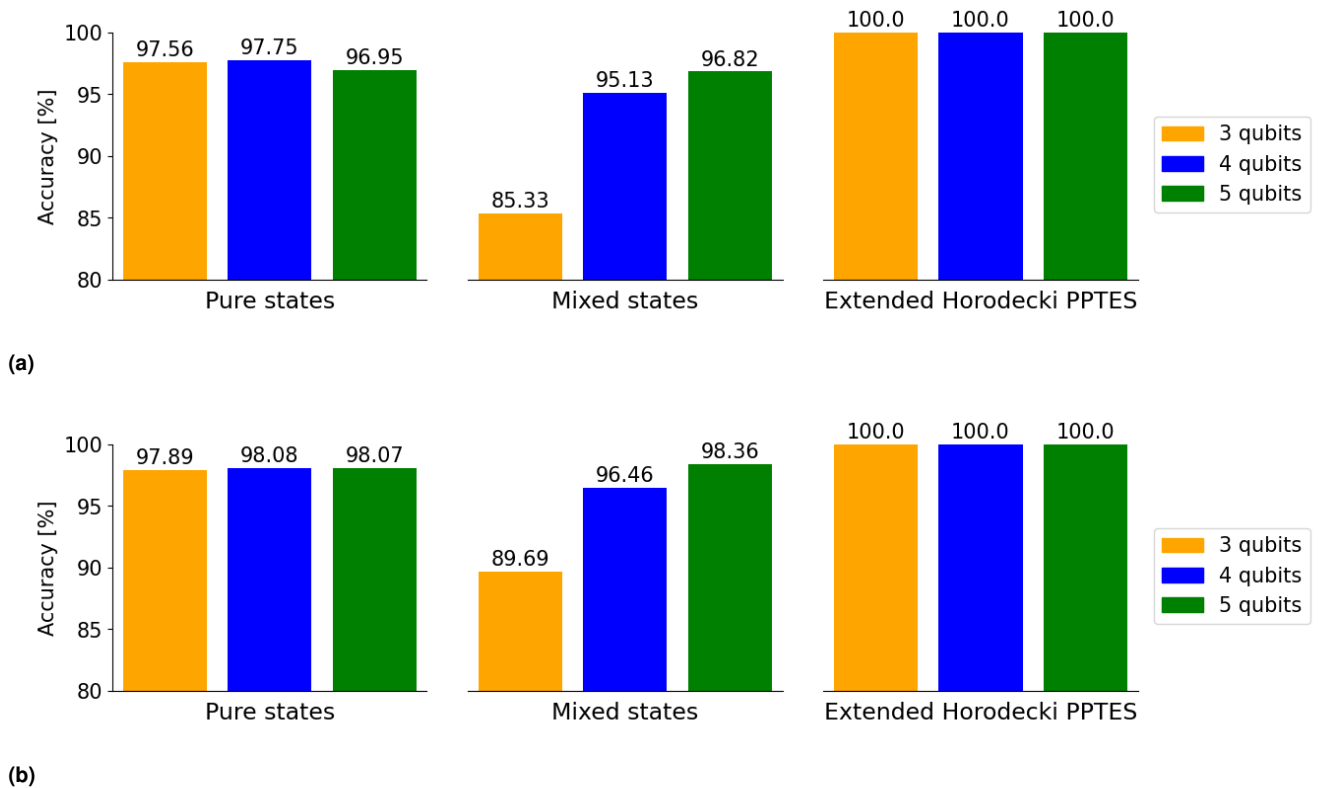


**Figure 4.** Accuracy of the models trained on the *weakly labeled* dataset for 3-, 4-, and 5-qubit systems in case of (a) CNN model, and (b) Siamese network.

as a backbone model instead of CNN, gave a worse performance. This shows that convolutional networks can be well suited to efficiently represent entanglement in multi-qubit systems. In addition, we were able to show that our model scales well to larger systems, ultimately obtaining average accuracy greater than 99%.

## Methods

To implement the quantum circuit model, during the training dataset generation, the python Qiskit<sup>45</sup> library is used. Also, when sampling from the uniform Haar measure during generation we use the built-in Qiskit method. Both the neural network models were implemented, trained, and evaluated using the PyTorch<sup>46</sup> library that supports autograd mechanism. The typical training time depends on the system size and ranges from 3-4 hours (CNN model) and 20 h (Siamese) for 3-qubit system, up to 5-6 h (CNN) and 30 h (Siamese) for 5-qubit. To train the neural network models we used Nvidia RTX 3070 GPU. The whole dataset generation lasts about 1 day for 3-qubit density matrices, to 4 days for 5-qubit ones, using typical few-core CPU.

## References

1. Krizhevsky, A., Sutskever, I. & Hinton, G. E. Imagenet classification with deep convolutional neural networks. *Adv. neural information processing systems* **25** (2012).
2. Ren, S., He, K., Girshick, R. & Sun, J. Faster r-cnn: Towards real-time object detection with region proposal networks. *Adv. neural information processing systems* **28** (2015).
3. Redmon, J., Divvala, S., Girshick, R. & Farhadi, A. You only look once: Unified, real-time object detection. In *Proceedings of the IEEE Conference on Computer Vision and Pattern Recognition (CVPR)* (2016).
4. Schroff, F., Kalenichenko, D. & Philbin, J. Facenet: A unified embedding for face recognition and clustering. In *Proceedings of the IEEE conference on computer vision and pattern recognition*, 815–823 (2015).
5. Carleo, G. & Troyer, M. Solving the quantum many-body problem with artificial neural networks. *Science* **355**, 602–606 (2017).

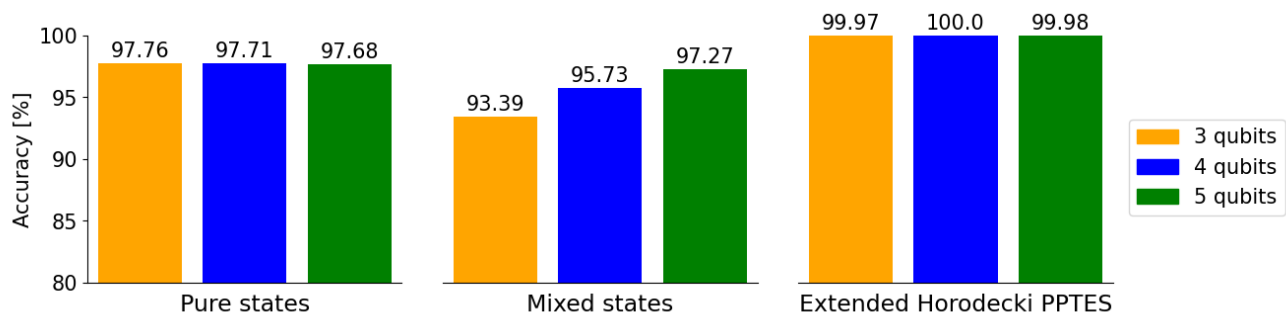


**Figure 5.** Accuracy of the Siamese network trained on the *verified* dataset for 3-, 4-, and 5-qubit systems.

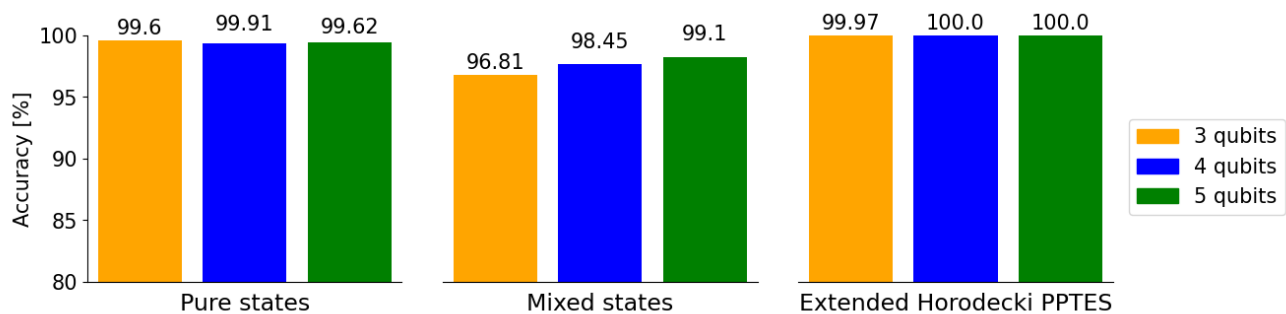


**Figure 6.** Final accuracy of the combined classifier consisting of negativity combined with the Siamese network for 3-, 4-, and 5-qubit systems.

6. Gao, X. & Duan, L.-M. Efficient representation of quantum many-body states with deep neural networks. *Nat. communications* **8**, 1–6 (2017).
7. Carleo, G., Nomura, Y. & Imada, M. Constructing exact representations of quantum many-body systems with deep neural networks. *Nat. communications* **9**, 1–11 (2018).
8. Tibaldi, S., Magnifico, G., Vodola, D. & Ercolessi, E. Unsupervised and supervised learning of interacting topological phases from single-particle correlation functions. *arXiv preprint arXiv:2202.09281* (2022).
9. Deng, D.-L., Li, X. & Das Sarma, S. Quantum entanglement in neural network states. *Phys. Rev. X* **7**, 021021, DOI: [10.1103/PhysRevX.7.021021](https://doi.org/10.1103/PhysRevX.7.021021) (2017).
10. Ma, Y.-C. & Yung, M.-H. Transforming bell's inequalities into state classifiers with machine learning. *npj Quantum Inf.* **4**, 1–10 (2018).
11. Levine, Y., Sharir, O., Cohen, N. & Shashua, A. Quantum entanglement in deep learning architectures. *Phys. review letters* **122**, 065301 (2019).
12. Carrasquilla, J. & Torlai, G. How to use neural networks to investigate quantum many-body physics. *PRX Quantum* **2**, 040201, DOI: [10.1103/PRXQuantum.2.040201](https://doi.org/10.1103/PRXQuantum.2.040201) (2021).
13. Bengtsson, I. & Życzkowski, K. *Geometry of quantum states: an introduction to quantum entanglement*, chap. Quantum entanglement (Cambridge University Press, 2017).
14. Plenio, M. B. & Virmani, S. S. *An Introduction to Entanglement Theory*, 173–209 (Springer International Publishing, Cham, 2014).
15. Horodecki, P. Separability criterion and inseparable mixed states with positive partial transposition. *Phys. Lett. A* **232**, 333–339, DOI: [10.1016/s0375-9601\(97\)00416-7](https://doi.org/10.1016/s0375-9601(97)00416-7) (1997).
16. Beer, K. *et al.* Training deep quantum neural networks. *Nat. Commun.* **11**, 808, DOI: [10.1038/s41467-020-14454-2](https://doi.org/10.1038/s41467-020-14454-2) (2020).
17. Yang, Z. & Zhang, X. Entanglement-based quantum deep learning. *New J. Phys.* **22**, 033041 (2020).
18. Schatzki, L., Arrasmith, A., Coles, P. J. & Cerezo, M. Entangled datasets for quantum machine learning. *arXiv preprint arXiv:2109.03400* (2021).
19. Cong, I., Choi, S. & Lukin, M. D. Quantum convolutional neural networks. *Nat. Phys.* **15**, 1273–1278, DOI: [10.1038/s41567-019-0648-8](https://doi.org/10.1038/s41567-019-0648-8) (2019).
20. Qiu, P.-H., Chen, X.-G. & Shi, Y.-W. Detecting entanglement with deep quantum neural networks. *IEEE Access* **7**, 94310–94320 (2019).
21. Banchi, L., Pancotti, N. & Bose, S. Quantum gate learning in qubit networks: Toffoli gate without time-dependent control. *npj Quantum Inf.* **2**, 16019, DOI: [10.1038/npjqi.2016.19](https://doi.org/10.1038/npjqi.2016.19) (2016).
22. Liu, Y. *et al.* Entanglement-based feature extraction by tensor network machine learning. *Front. Appl. Math. Stat.* **7**, DOI: [10.3389/fams.2021.716044](https://doi.org/10.3389/fams.2021.716044) (2021).
23. Chen, Y., Pan, Y., Zhang, G. & Cheng, S. Detecting quantum entanglement with unsupervised learning. *Quantum Sci. Technol.* **7**, 015005, DOI: [10.1088/2058-9565/ac310f](https://doi.org/10.1088/2058-9565/ac310f) (2021).
24. Goes, C. B., Canabarro, A., Duzzioni, E. I. & Maciel, T. O. Automated machine learning can classify bound entangled states with tomograms. *Quantum Inf. Process.* **20**, 1–18 (2021).
25. Lu, S. *et al.* Separability-entanglement classifier via machine learning. *Phys. Rev. A* **98**, 012315, DOI: [10.1103/PhysRevA.98.012315](https://doi.org/10.1103/PhysRevA.98.012315) (2018).
26. Życzkowski, K., Horodecki, P., Sanpera, A. & Lewenstein, M. Volume of the set of separable states. *Phys. Rev. A* **58**, 883–892, DOI: [10.1103/PhysRevA.58.883](https://doi.org/10.1103/PhysRevA.58.883) (1998).
27. Peres, A. Separability criterion for density matrices. *Phys. Rev. Lett.* **77**, 1413–1415, DOI: [10.1103/PhysRevLett.77.1413](https://doi.org/10.1103/PhysRevLett.77.1413) (1996).
28. Horodecki, M., Horodecki, P. & Horodecki, R. Separability of mixed states: necessary and sufficient conditions. *Phys. Lett. A* **223**, 1–8, DOI: [https://doi.org/10.1016/S0375-9601\(96\)00706-2](https://doi.org/10.1016/S0375-9601(96)00706-2) (1996).
29. Wootters, W. K. Entanglement of formation of an arbitrary state of two qubits. *Phys. Rev. Lett.* **80**, 2245–2248, DOI: [10.1103/PhysRevLett.80.2245](https://doi.org/10.1103/PhysRevLett.80.2245) (1998).
30. Carvalho, A. R. R., Mintert, F. & Buchleitner, A. Decoherence and multipartite entanglement. *Phys. Rev. Lett.* **93**, 230501, DOI: [10.1103/PhysRevLett.93.230501](https://doi.org/10.1103/PhysRevLett.93.230501) (2004).

31. Lewenstein, M., Kraus, B., Cirac, J. I. & Horodecki, P. Optimization of entanglement witnesses. *Phys. Rev. A* **62**, 052310, DOI: [10.1103/PhysRevA.62.052310](https://doi.org/10.1103/PhysRevA.62.052310) (2000).
32. Bengtsson, I. & Życzkowski, K. Geometry of quantum states: An introduction to quantum entanglement. *Geom. Quantum States: An Introd. to Quantum Entanglement* DOI: [10.1017/CBO9780511535048](https://doi.org/10.1017/CBO9780511535048) (2006).
33. Doherty, A. C., Parrilo, P. A. & Spedalieri, F. M. Distinguishing separable and entangled states. *Phys. Rev. Lett.* **88**, DOI: [10.1103/physrevlett.88.187904](https://doi.org/10.1103/physrevlett.88.187904) (2002).
34. Hulpke, F. & Bruß, D. A two-way algorithm for the entanglement problem. *J. Phys. A: Math. Gen.* **38**, 5573–5579, DOI: [10.1088/0305-4470/38/24/011](https://doi.org/10.1088/0305-4470/38/24/011) (2005).
35. Liang, X., Dong, S.-J. & He, L. Hybrid convolutional neural network and projected entangled pair states wave functions for quantum many-particle states. *Phys. Rev. B* **103**, 035138, DOI: [10.1103/PhysRevB.103.035138](https://doi.org/10.1103/PhysRevB.103.035138) (2021).
36. Choo, K., Neupert, T. & Carleo, G. Two-dimensional frustrated  $J_1$ – $J_2$  model studied with neural network quantum states. *Phys. Rev. B* **100**, 125124, DOI: [10.1103/PhysRevB.100.125124](https://doi.org/10.1103/PhysRevB.100.125124) (2019).
37. Broecker, P., Carrasquilla, J., Melko, R. G. & Trebst, S. Machine learning quantum phases of matter beyond the fermion sign problem. *Sci. Reports* **7**, 8823, DOI: [10.1038/s41598-017-09098-0](https://doi.org/10.1038/s41598-017-09098-0) (2017).
38. Roth, C. & MacDonald, A. H. Group convolutional neural networks improve quantum state accuracy. *arXiv preprint arXiv:2104.05085* (2021).
39. Mezzadri, F. How to generate random matrices from the classical compact groups. *Notices Am. Math. Soc.* **54** (2006).
40. Cruz, D. *et al.* Efficient quantum algorithms for ghz and w states, and implementation on the ibm quantum computer. *Adv. Quantum Technol.* **2**, 1900015, DOI: <https://doi.org/10.1002/qute.201900015> (2019). <https://onlinelibrary.wiley.com/doi/pdf/10.1002/qute.201900015>.
41. Tura, J. *et al.* Four-qubit entangled symmetric states with positive partial transpositions. *Phys. Rev. A* **85**, 060302, DOI: [10.1103/PhysRevA.85.060302](https://doi.org/10.1103/PhysRevA.85.060302) (2012).
42. Acín, A., Bruß, D., Lewenstein, M. & Sanpera, A. Classification of mixed three-qubit states. *Phys. Rev. Lett.* **87**, DOI: [10.1103/physrevlett.87.040401](https://doi.org/10.1103/physrevlett.87.040401) (2001).
43. Bennett, C. H. *et al.* Unextendible product bases and bound entanglement. *Phys. Rev. Lett.* **82**, 5385–5388, DOI: [10.1103/PhysRevLett.82.5385](https://doi.org/10.1103/PhysRevLett.82.5385) (1999).
44. Roberts, C. *et al.* TensorNetwork: A library for physics and machine learning (2019). [1905.01330](https://doi.org/10.26434/chemrxiv-2019-01330).
45. Abraham, H. *et al.* Qiskit: An open-source framework for quantum computing, DOI: [10.5281/zenodo.2562110](https://doi.org/10.5281/zenodo.2562110) (2019).
46. Paszke, A. *et al.* Pytorch: An imperative style, high-performance deep learning library. In Wallach, H. *et al.* (eds.) *Advances in Neural Information Processing Systems* **32**, 8024–8035 (Curran Associates, Inc., 2019).

# Supplementary Materials

## Circuit for random states generation

Here we present two methods for generating random pure states.

The first idea is to use a quantum circuit model. It is a common technique in the quantum computing, when one needs to process states of many qubits. In this approach, firstly we initialize the set (register) of  $N$  qubits in a given state (usually  $|0\rangle^{\otimes N}$ ), and then apply so-called quantum gates. One can distinguish two main types of such operations: the local – single-qubit gates, and the two-qubit controlled gates. Although both of them can be understood as rotations on the qubit sphere by the given angles, in the latter such operation is performed only on the single qubit while the rest of qubits can be used to determine (control) whether this operation should or should not be performed. Controlled gate can be used to entangle two qubits. In contrast, single qubit gates can only modify the local states of qubits and not influence the global entanglement properties. Therefore, combining these two types of quantum gates with appropriate parameters (angles), one can obtain a suitable generator of pure states, both entangled and separable ones. The universal single qubit gate is defined as follows:

$$U(\theta, \phi, \lambda) = \begin{pmatrix} \cos \frac{\theta}{2} & -e^{i\lambda} \sin \frac{\theta}{2} \\ e^{i\phi} \sin \frac{\theta}{2} & e^{i(\phi+\lambda)} \cos \frac{\theta}{2} \end{pmatrix}, \quad (\text{SM1})$$

where  $\theta$ ,  $\phi$  and  $\lambda$  are three Euler angles. Subsequently, the controlled universal gate is described as:

$$CU(\theta, \phi, \lambda, \gamma) = \begin{pmatrix} 1 & 0 & 0 & 0 \\ 0 & 1 & 0 & 0 \\ 0 & 0 & e^{i\gamma} \cos \frac{\theta}{2} & -e^{i(\gamma+\lambda)} \sin \frac{\theta}{2} \\ 0 & 0 & e^{i(\gamma+\phi)} \sin \frac{\theta}{2} & e^{i(\gamma+\phi+\lambda)} \cos \frac{\theta}{2} \end{pmatrix}, \quad (\text{SM2})$$

with additional global phase  $e^{i\gamma}$ . To obtain the most possible diversified dataset, the parameters of these two gates are chosen at random, where the range for the each parameter  $\theta$ ,  $\phi$ ,  $\lambda$ , and  $\gamma$  is equal to  $[0, 2\pi)$ .

Let us now describe the circuit organization. At first, the system is initialized in the random separable state by applying the  $U$  gates to each of qubit in the register. Next, the random number of  $CU$  gates is picked from the range  $[1, 2\binom{N}{2})$ , where  $N$  is the number of qubits. The  $CU$  gates are put to random pairs of qubits. And finally, the state is locally randomized, again, by applying the  $U$  gates.

The second idea of generating random pure states is based on sampling from the uniform Haar measure. At first, we generate a vector  $\mathbf{x}$  of size  $K = 2^N$  ( $N$  is the number of qubits) with its elements being uniformly sampled over an interval  $(0, 1]$ . Secondly, we replace each coordinate  $x_i$  with  $y_i = -\log(x_i)$ , therefore obtaining vector  $\mathbf{y}$  with logarithmic distribution over an interval  $[0, \infty)$ . Next, we generate a  $K$ -dimensional phase vector  $\boldsymbol{\gamma}$ , where each coordinate is chosen at random from the range  $[0, 2\pi)$ . Finally we construct a state vector as:

$$|\Psi_{\text{Haar}}\rangle = \sqrt{\frac{y_1}{\sum_i y_i}} e^{i\gamma_1} |00\dots 0\rangle + \dots + \sqrt{\frac{y_K}{\sum_i y_i}} e^{i\gamma_K} |11\dots 1\rangle. \quad (\text{SM3})$$

## Strategies for states labeling

We propose three different strategies for labeling PPT mixed states, i.e. in situation where negativity criterion is inconclusive.

The most simple solution is to trust negativity metric and always label mixed state accordingly to the  $Neg$  value – we will call this strategy as *negativity labeled*. However, such approach may result in a network trained to reflect just the PPT criterion instead of actual entanglement. That is why we can think of the second method, which simply excludes mixed PPT states (with  $Neg = 0$ ). We will call this strategy as *verified*, because all the labels here are again correct. The main disadvantage of such a solution is that it automatically excludes all of mixed separable states from the training set. To minimize this drawback, we generate some extra mixed separable states straight from the definition:

$$\rho_{abc} = \sum_i p_i \rho_a^i \otimes \rho_b^i \otimes \rho_c^i, \quad (\text{SM4})$$

where one can generate single qubit states  $\rho_a^i, \rho_b^i, \rho_c^i$ , and combine them with Kronecker product into 3-qubits mixed separable state  $\rho_{abc}$ . This approach can be easily generated for  $N$ -qubit states just by extending the number of single qubit states.

Finally, we propose the third solution for labeling mixed states, which extends the second method in a way that PPT states are not excluded, but an additional labeling criterion is applied to them. Control gates play a significant role in circuit based

generation method since they introduce entanglement between two qubits, which are connected by such gate. Following this logic, if we generate larger pure state and then take a partial trace of it in such a way, that remaining qubits are directly connected by a control gate  $CU$ , we can suppose, that we likely obtain an entangled mixed state. Specifically, for each bipartition  $A|B$  of the mixed state  $\rho_{AB}$ , if there is a control gate, which connects qubits  $a$  and  $b$ , where  $a \in A$  and  $b \in B$ , then we label this bipartition as entangled. We call this third mixed states labeling strategy as *weakly labeled* because there is no guarantee that such labels are always correct.

## Generated datasets structure

Having three strategies for labeling mixed states (labeling pure states is obvious), we consider generating separate training datasets, each corresponding to the different strategy: *negativity labeled*, *verified*, and *weakly labeled*. All of them retain the same structure of pure states: 40 000 pure separable states, and 60 000 pure entangled states – generated using random circuits (using  $U$  (Eq. SM1) and  $CU$  (Eq. SM2) gates) including W and GHZ, and sampling from Haar measure method (Eq. SM3).

In case of mixed states we generate 60 000 mixed separable states using separable circuits and formula (Eq. SM4). We also add 20 000 separable states generated as a Kronecker product of mixed single-qubit states obtained by tracing from the larger system. Then, we generate 90 000 mixed entangled states by mixing pure entangled states explicitly from the definition (Eq. 7), and keeping only those with  $Neg > 0$  (NPT). Finally, we add 60 000 mixed states generated with the use of the partial trace from a global pure entangled state (Eq. 8). For the last group (the data generated with the use of quantum circuits) in which we have no guarantee that states are either separable or entangled, we apply the three labeling strategies. This latter group is important because it contains PPTES, and therefore allows to train a model to capture them. Contrarily, the states generated by sampling from the Haar measure are always verified and kept only when  $Neg > 0$ . All in all, the training set contains 330 000 samples.

In order to correctly evaluate the model, apart from the training sets, the validation and test sets were also created. The validation set is generated with the same distribution as the verified training set but with reduced number of examples, i.e. 10% meaning 33 000 states generated. Next, we defined two test datasets for pure and mixed states separately. The former consists of 15 000 separable states, (separable circuits and Kronecker product of single qubit states), and 15 000 entangled states (random circuits and sampling from Haar measure). The latter contains 20 000 separable states (mixture of separable circuits and Kronecker product), and 20 000 entangled containing NPT states only, generated both from the definition (Eq. 7) and using partial trace (Eq. 8). One important note is that while for the training and validation sets the maximal number of pure states  $d$  included in the mixture (Eq. 7) is set to  $2^N$ , it is no longer true for test sets. As for them, in order to properly capture the behaviour of PPT/NPT transition in the regime of  $d$ , which will be analyzed in the next section, let us explicitly set the maximal values of  $d$  to 30, 70 and 190 respectively for 3, 4 and 5-qubit systems. Such border values guarantee that at least 10% of states, generated from the mixture of fully-entangled pure states, are NPT (see Figs. Figs. 2 and 3).

## Networks architecture optimization

Having defined the CNN and the extended Siamese network model, we optimized their architecture hyperparameters by training them on the weakly labeled training set and evaluating on the validation set. In particular, each model was trained for 20 epochs. Then, we measured the averaged bipartition accuracy of the model on the validation set for each epoch separately and finally we chose the most accurate model among all of the epochs.

Having performed the above procedure for different models, we can compare their architectures and consequently find the most optimal one. This is demonstrated in Fig. 1, where the accuracy for the CNN and Siamese network models is plotted against the kernel size in the convolutional layer. One can also notice, that using deeper (consisting of more layers) models tend to have better accuracy, especially when choosing the right kernel size. One important remark is, that using deeper model and no padding automatically reduces the maximal kernel size, which can be used. That is why in case of model with 3 convolutional layers, the maximal kernel size for 3-qubits systems ( $8 \times 8$  density matrix) is equal to  $3 \times 3$ . Moreover, using deeper model results in much longer training time, especially for systems with more qubits. Therefore, also in that case, we limit our tests to 3 convolutional layers only. Analyzing the obtained results, one can clearly see that the most efficient architecture is the Siamese network with 3 convolutional layers and kernel size equal to  $2 \times 2$ . Hence, in the Results section in the main text we are sharing outcomes mainly for such a model, although some comparisons to the standard CNN model are also provided.

## Training set impact on various-sized systems

The dependence on the method used to label states in the training sets can be further analyzed by investigating the difference of the models predictions with the negativity-based predictions, i.e. predictions made using the negativity calculated for the

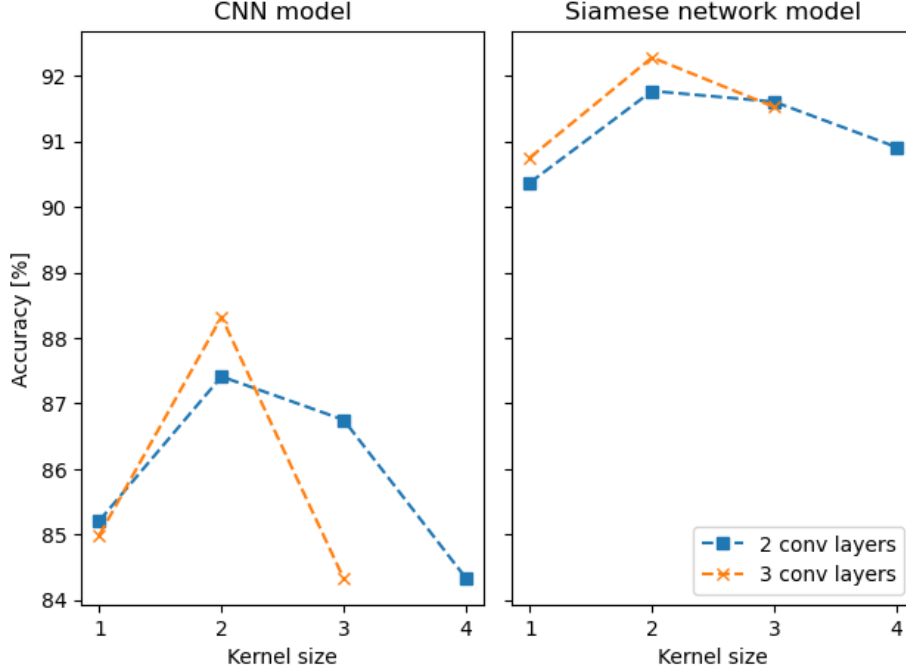


**Figure 1.** Architecture optimization for the 3-qubit system. Siamese network and CNN models were trained on the *weakly labeled* dataset and verified using the validation dataset.

actually analyzed state. Precisely, one can define this difference as:

$$\Delta Neg = \frac{1}{mn} \sum_j^m \sum_i^n |p_j(\rho_i) - p_j^{Neg}(\rho_i)|, \quad (\text{SM5})$$

where by  $p_j(\rho_i)$  we denote the neural network prediction if the state  $\rho_i$  is entangled in bipartition  $j$ , while  $p_j^{Neg}(\rho_i)$  represents the negativity prediction for the same state  $\rho_i$  and bipartition  $j$ . To normalize this value, we divide it by the total number of data samples  $n$  and bipartitions  $m$ . Then, by defining the *Convergence with Negativity*:

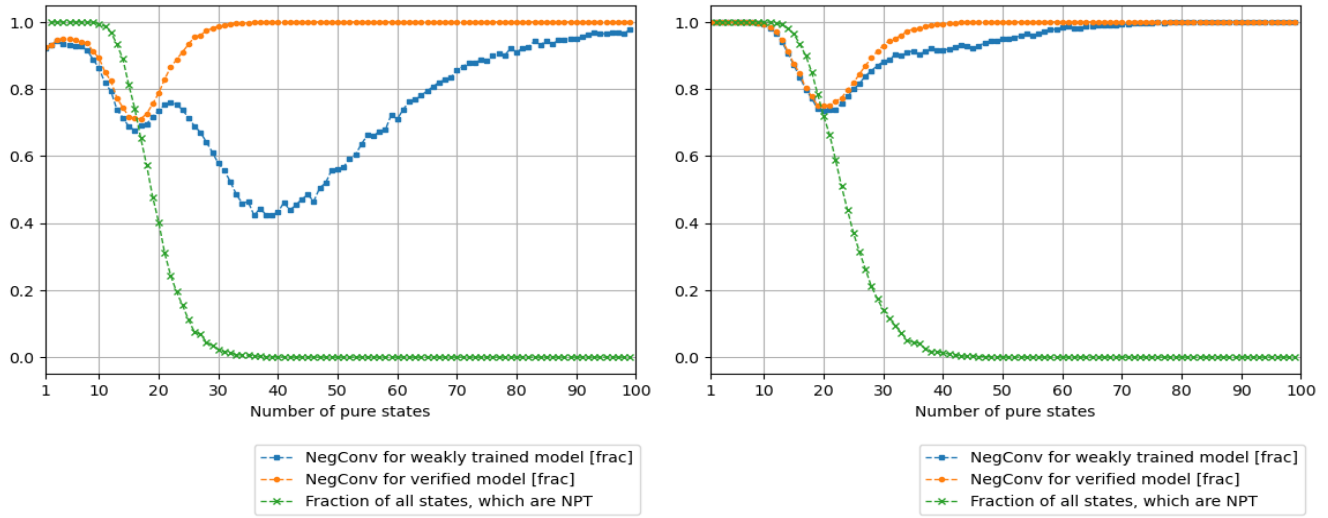
$$ConvNeg = 1 - \Delta Neg, \quad (\text{SM6})$$

we arrive at quantity which just describes how many predictions are the same as negativity. In case of NPT states, or mixed separable states constructed straight from the definition (Eq. SM4), *ConvNeg* is equivalent to the accuracy of bipartite entanglement detection (Eq. 9).

In Fig. 2(a) there are presented results for 3-qubit Siamese model (same as from Table 3) trained on the *weakly labeled*, and *verified* sets. We can observe that using *weakly labeled* training set (blue curve), where some PPT states are labeled as entangled, results in existence of two local minima of *ConvNeg*. The first one overlaps with the minimum corresponding to *verified* dataset (orange curve). Both curves are plotted for different test sets, defined with different number  $d$  of pure states in the mixture (Eq. 7). What is interesting, the fraction of NPT states in these test sets (green curve) sharply depends on  $d$ . This transition-like behaviour slightly depends on the method used to generate pure states (circuit- vs. Haar-generated) used in the mixture. The second minimum of *ConvNeg* appears in the regime of PPT states ( $d > 30$ ), which indicates that neural network learned also some other pattern differing between separable and entangled states. However, if we also plot the accuracy for another set containing mixtures of pure separable states, presented in Fig. 2(b), one can immediately see, that this second minimum occurs also in this case. Hence, it proves that network has learned some artifact, which is not useful in recognizing entanglement. Therefore, one should decide to use the *verified* method for labeling the data in the case of 3-qubit systems.

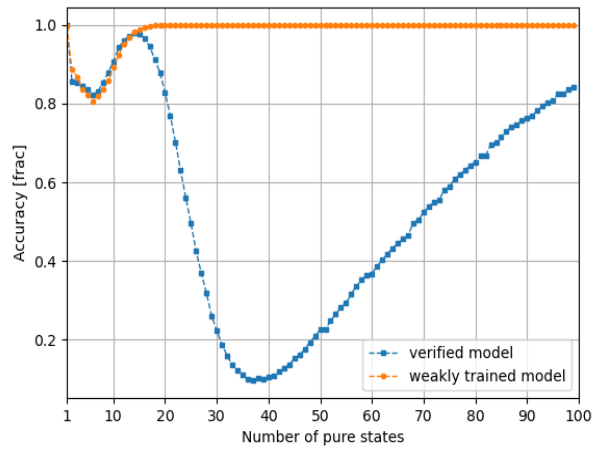
On the other hand, for larger systems, the network tends to achieve better accuracy when training on the *weakly labeled* – see Fig. 3 with results for 4-qubit system. It is noticeable, that for mixture of both pure entangled and pure separable states there is only one minimum – see Fig. 3. Moreover, in case of mixture of entangled states – Fig. 3(a), the minimum of *ConvNeg* for the network trained on the *weakly labeled* dataset (blue curve) is shifted to PPT states regime. It may suggest, that such a network is able to detect some PPTES, which are not detected by the network trained on the *verified dataset*. Moreover, in case

of mixture of separable states – Fig. 3(b), the accuracy of the former network (blue curve) decreased less than for the latter one (orange), hence, resulting in the higher overall accuracy. That is why, we propose to use the *verified* dataset only to train the network in case of 3-qubit system, while switch to *weakly labeled* for higher dimensional spaces. We verified that for the 5-qubit system the results are similar, with better accuracy for the *weakly labeled* training set, but the number of pure states needed to get transition from NPT to PPT (green curve in Figs. 2 and 3) shifts toward a higher number of pure states.



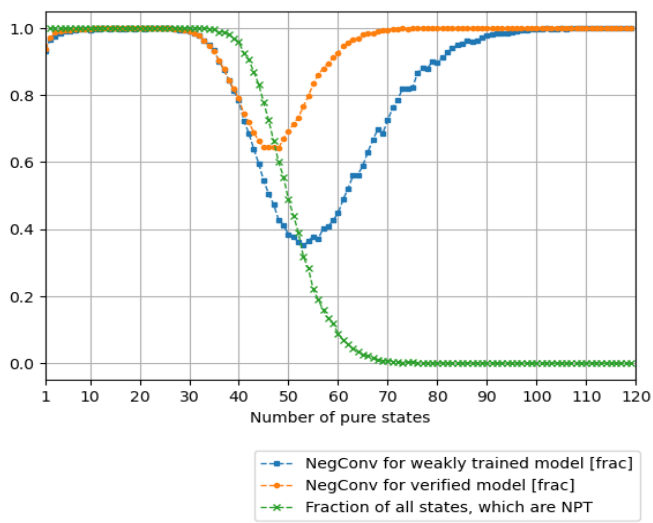
(a)

(b)

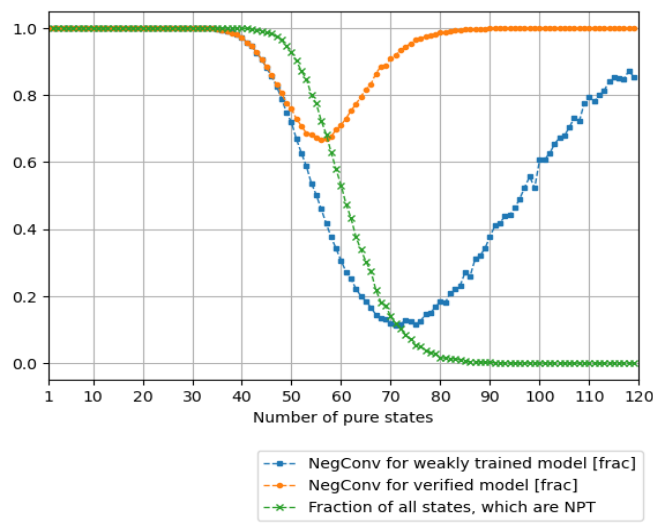


(c)

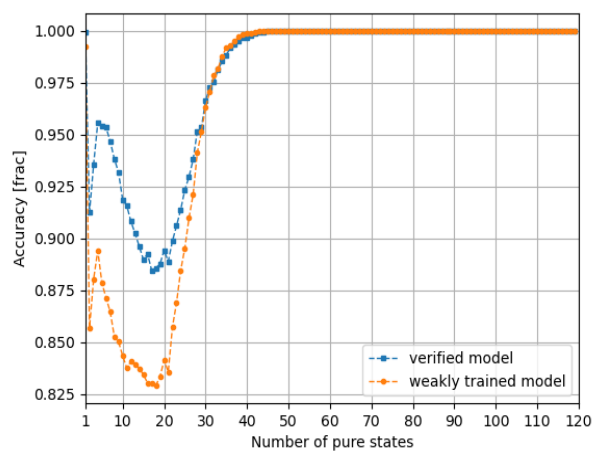
**Figure 2.** Convergence with negativity for predictions made by 3-qubit Siamese network for test sets consisting of states mixed from different number of pure states. The results are presented for models trained on *weakly labeled* set (blue curve) and *verified* dataset (orange curve). In addition, the fraction of states which are NPT is also presented (green curve). Mixture of fully entangled pure states is plotted separately for circuit generated density matrices (a), and those sampled from Haar measure (b). Mixture of separable pure states composed of both circuit and Haar-like generated samples (c).



(a)



(b)



(c)

**Figure 3.** Same as in Fig. 2 but for larger, 4-qubit system.